RESEARCH ARTICLE

WILEY

Intracortical brain-heart interplay: An EEG model source study of sympathovagal changes

Vincenzo Catrambone[1] | Diego Candia-Rivera[2] | Gaetano Valenza[1]

[1]Neurocardiovascular Intelligence Laboratory & Department of Information Engineering & Bioengineering and Robotics Research Center, E. Piaggio, School of Engineering, University of Pisa, Pisa, Italy

[2]Sorbonne Université, Paris Brain Institute (ICM), INRIA, CNRS, INSERM, AP-HP, Hôpital Pitié-Salpêtrière, Paris, France

Correspondence
Vincenzo Catrambone, Neurocardiovascular Intelligence Laboratory & Department of Information Engineering & Bioengineering and Robotics Research Center, E. Piaggio, School of Engineering, University of Pisa, Pisa, Italy.
Email: vincenzo.catrambone@ing.unipi.it

Abstract

The interplay between cerebral and cardiovascular activity, known as the functional brain-heart interplay (BHI), and its temporal dynamics, have been linked to a plethora of physiological and pathological processes. Various computational models of the brain-heart axis have been proposed to estimate BHI non-invasively by taking advantage of the time resolution offered by electroencephalograph (EEG) signals. However, investigations into the specific intracortical sources responsible for this interplay have been limited, which significantly hampers existing BHI studies. This study proposes an analytical modeling framework for estimating the BHI at the source-brain level. This analysis relies on the low-resolution electromagnetic tomography sources localization from scalp electrophysiological recordings. BHI is then quantified as the functional correlation between the intracortical sources and cardiovascular dynamics. Using this approach, we aimed to evaluate the reliability of BHI estimates derived from source-localized EEG signals as compared with prior findings from neuroimaging methods. The proposed approach is validated using an experimental dataset gathered from 32 healthy individuals who underwent standard sympathovagal elicitation using a cold pressor test. Additional resting state data from 34 healthy individuals has been analysed to assess robustness and reproducibility of the methodology. Experimental results not only confirmed previous findings on activation of brain structures affecting cardiac dynamics (e.g., insula, amygdala, hippocampus, and anterior and mid-cingulate cortices) but also provided insights into the anatomical bases of brain-heart axis. In particular, we show that the bidirectional activity of electrophysiological pathways of functional brain-heart communication increases during cold pressure with respect to resting state, mainly targeting neural oscillations in the δ, β, and γ bands. The proposed approach offers new perspectives for the investigation of functional BHI that could also shed light on various pathophysiological conditions.

KEYWORDS
Brain-Heart, EEG, heart rate variability, source analysis

Vincenzo Catrambone and Diego Candia-Rivera contributed equally to this work.

1 | INTRODUCTION

Characterization of the complex phenomena underlying the functional relationship between the central nervous system (CNS) and autonomic nervous system (ANS) has increasingly gained attention in the last decade. Although initially believed to pertain solely to central control over peripheral organs, the phenomenon is multi-faceted and can be studied at different scales, from neural and glial signaling (Marina et al., 2016; Truter et al., 2023) to functional psychosomatic reverberations (Candia-Rivera, Catrambone, Thayer, et al., 2022; Skora et al., 2022).

The study of central-autonomic interplay has placed particular emphasis on studying cardiac dynamics because of their ease of measurement and connection to both the sympathetic and parasympathetic nervous systems (Chen et al., 2021; Liu et al., 2022). In this context, most functional brain-heart interplay (BHI) estimations have been performed using noninvasive electrophysiological signals, specifically EEG and heart rate variability (HRV) series. Notably, these approaches offer a sufficiently high time resolution, which is a crucial factor, given the time-varying nature of BHI. The variety of physiological and clinical contexts in which BHI is involved reflects its importance (Benarroch, 1993; Catrambone & Valenza, 2021; Schiecke et al., 2016; Silvani et al., 2016; Valenza et al., 2020; Valenza et al., 2024).

Indeed, several methodologies have emerged for estimating the BHI, addressing different aspects, such as directionality, synchronization, and complexity. These include formulation of an ad hoc synthetic data-generation model (Candia-Rivera, 2023; Candia-Rivera, Catrambone, Barbieri, & Valenza, 2022; Catrambone et al., 2019; Catrambone, Talebi, et al., 2021), the application of information theory to disentangle linear and nonlinear components (Faes et al., 2015) and to quantify information storage (Antonacci et al., 2023; Barà et al., 2023), nervous system—wise functional estimation through microstate occurrences (Catrambone & Valenza, 2023b), or methods exploiting state-space reconstruction to investigate nonlinear and directed interactions (Schiecke et al., 2016).

Currently proposed EEG-derived techniques excel in investigating time-resolved BHI processes with optimal time resolution, but they are limited in terms of the spatial domain. Nevertheless, the efferent and afferent functional pathways of ANS activity involve several cortical and subcortical regions of the CNS, which form part of the central autonomic network (CAN) (Benarroch, 1993; Benarroch, 2012). Indeed, limbic structures, such as the cingulate cortex, medial temporal lobe, amygdala, and hippocampus, and regions such as the ventral medial prefrontal, insular, and parietal cortices are associated with autonomic responses, and these regions all belong to the CAN (Benarroch, 1993; Catrambone & Valenza, 2021; Valenza et al., 2019). The identification of CAN components has primarily been attained through technologies such as functional magnetic resonance imaging (fMRI), which allows investigation of the activity of deep CNS regions with commendable spatial resolution at the cost of a temporal resolution that is inferior to that of EEG.

Source localization of EEG signals aims to solve the inverse problem of accurately estimating the brain regions that trigger electromagnetic changes measured at the scalp level by leveraging spatial modeling of electrical propagation in brain tissues. This depends on a variety of factors, including the neurophysiology of EEG sources, biophysics of electrical propagation, anatomy of conductive tissues, and neuronal activity distribution properties (Michel & He, 2019). To this extent, new source estimation methodologies have been developed based on the most recent knowledge of EEG signal generation. The first method for resolving the EEG inverse problem involves localization of a constrained set of equivalent dipoles. According to the traditional method of dipole source localization, the scalp potential field is produced by only one or a few active brain regions. Nonlinear optimization can be used to identify a mathematically ideal solution under this restriction. Epileptic foci or primary sensory areas, such as the sensorimotor cortex in surgical candidates, can be located with reasonable results using dipole source localization, despite the simplicity and limitations of this a priori assumption. Distributed-source imaging approaches have largely replaced dipole source localization in experimental EEG studies. In this case, a large number of equivalent dipoles (order of magnitude of ≈ 5000) are dispersed in fixed locations across the entire source space, and the strength of each dipole is estimated (Michel & He, 2019). The source space is typically limited to the grey matter, using an individual's anatomical information or template MRI. One of the most commonly used methods is low-resolution electromagnetic tomography (LORETA), developed by (Pascual-Marqui et al., 1994). LORETA and its variations (e.g., sLORETA (Pascual-Marqui et al., 2002)) rely on the minimization of the Laplacian operator of the sources, resulting in a smooth (low resolution) distribution of 3D activity. This constraint is justified by the physiologically tenable hypothesis that the activity in adjacent voxels is correlated. In this study, we employed *sLORETA* (Pascual-Marqui et al., 2002) as a source localization technique. While it is a widely utilized method, it achieves very good performance in localizing electrical activity sources, has small computational complexity, provides a closed-form expression based on an L2-norm-based solution, and is available in the form of an open-source toolbox/library. Further information on source localization methodologies proposed in the literature can be found in, for example, (Asadzadeh et al., 2020).

Previous studies investigated the intracranial activity using invasive stereo-EEG-based heartbeat-evoked potentials (HEPs) (Mazzola et al., 2023). HEPs are calculated by averaging the sEEG signals that synchronize with the R peaks of the concurrent ECG signal (Park & Blanke, 2019). These studies indicated that HEPs originate from specific brain regions, including the anterior cingulate, right insula, prefrontal cortex, and left secondary somatosensory cortex (Babo-Rebelo et al., 2016; Park et al., 2018; Park & Blanke, 2019), which are known to interact with emotional, cognitive, and sensory processing. However, this approach comes with limitations (Park & Blanke, 2019). First, the stereo-EEG recordings are invasive and may not be easily gathered from the general population. Second, cardiac electric currents associated with ventricular contractions might induce artifacts in stereo-EEG signals that can bias the HEP assessment. Third, cardiac

cycle is influenced by dynamical variations in sympathetic and para-sympathetic autonomic activities, which might be linked to several EEG oscillations in an afferent and efferent fashion. Therefore, a comprehensive understanding of key cortical and sub-cortical regions involved in cardiac autonomic control, that is, the functional brain-heart axis, using non-invasive techniques is yet to be achieved.

In this study, we investigated the reliability of markers of functional BHI estimated from intracortical source-localized signals and cardiac sympathovagal oscillations. To the best of our knowledge, no previous study has endeavored to estimate BHI through a functional correlation between EEG model sources and cardiovascular activity.

To validate the proposed methodology, we tested it on data gathered during a cold pressor test (CPT), which is a well-known autonomic maneuver involving thermal stress that elicits a strong sympathovagal response (Cui et al., 2002). Physiological responses associated with thermal and nociceptive stress include increased heart rate, which is attributed to higher sympathetic activity and lower vagal outflow. At the CNS level, brain correlates of the CPT include cortical and subcortical brain activation, such as an increase in power in the delta and gamma bands in the fronto-temporal areas (Chang et al., 2002; Fardo et al., 2017; Shao et al., 2012). Additionally, our previous studies on functional BHI dynamics during the CPT have revealed a bidirectional and diffuse interaction (Catrambone & Valenza, 2023a; Catrambone & Valenza, 2023b) with changes predominantly in the EEG gamma and delta bands (Candia-Rivera, Catrambone, Barbieri, & Valenza, 2022; Catrambone et al., 2019), which were directly connected to ascending communication pathways from autonomic inputs and corroborated by changes in HEPs (Shao et al., 2011).

2 | MATERIALS AND METHODS

2.1 | Dataset description

The first dataset (D1) came from a group of 32 right-handed young healthy adults underwent a CPT while recording physiological signals. Data from 26 subjects (age range, 21–41 years; median, 27 years; 13 males) were considered for further analysis because of data length and quality. In particular, data from three subjects were not considered because of the presence of artifacts in their physiological data (EEG or ECG), while data from three subjects were discarded because of early withdrawal of their hands from the cold water. Each subject's recording comprised of a 128-channel high-density EEG (Electrical Geodesics, Inc., Eugene, OR, USA), respiratory activity, and one-lead ECG, sampled at 500 Hz. Before data acquisition, the subjects were asked to sit comfortably on a chair to ensure hemodynamic stabilization. Throughout the protocol, subjects were asked to keep their eyes closed to minimize artifacts. The task consisted of a 3-min resting state, followed by a 3-min CPT, in which the subjects were guided to submerge their left hand up to the write into asked place their hand into a bucket filled with ice water (0–4°C), and a recovery phase, in which subjects were asked to withdraw their hand from the ice-water bucket.

To better assess robustness and reliability of the experimental results, a second dataset (D2) has been considered. It consisted of physiological signals recordings (EEG and ECG) gathered employing the same devices of the first dataset on a group of 34 healthy right-handed young subjects (age range, 26.5 years median; 18 males, there were no subject in common between the two groups) performing a 3 min resting state in a dark room. The same dataset has been already presented and analysed in previous studies (Catrambone, Averta, et al., 2021), and is part of a larger experiment whose data are freely available (Averta et al., 2021).

2.2 | EEG processing

EEG data were preprocessed using MATLAB R2017a and the Fieldtrip Toolbox (Oostenveld et al., 2011). The data were bandpass filtered with a Butterworth filter of order four, between 0.5 and 45 Hz. Large-movement artifacts were removed using wavelet-enhanced independent component analysis (ICA) (Gabard-Durnam et al., 2018), which were identified using automated thresholding over the independent component and multiplied by 50 to remove only very large artifacts, as described by Candia-Rivera et al. (2021). Consequently, ICA was re-run to recognize and reject eye movements and cardiac-field artifacts from the EEG data (Dirlich et al., 1997). Therefore, a one-lead ECG was included as an additional input to the ICA to enhance the process of identifying cardiac artifacts. Once the ICA components with eye movements and cardiac artifacts were visually identified, they were set to zero to reconstruct the EEG series. This step thus yielded eye movement- and cardiac artifact-free EEG data. Individual EEG channels were analyzed. The channels were marked as contaminated if their area under the curve exceeded three standard deviations of the mean for all channels. The remaining channels were compared with their weighted-by-distance-correlation neighbors using the standard field-trip neighbor' definition. If a channel resulted in a weighted-by-distance correlation of less than 0.6, it was considered contaminated. The contaminated channels were replaced by neighbor' interpolation. The channels were referenced using a common average, which is the most appropriate for a functional BHI assessment (Candia-Rivera et al., 2021).

2.3 | EEG source localization

Source-level analysis was performed on EEG at −60 to 60 s with respect to the cold-pressure onset for the first dataset, and an homogeneous time window of 60 s was taken for dataset 2 as well. The source reconstruction was performed using the Brainstorm toolbox (Tadel et al., 2011). Default anatomy (ICBM152) was used together with EGI 128 electrode locations. A three-shell sphere was created for each participant using no-noise modeling, and sources were computed using default parameters (minimum norm imaging, sLORETA method, constrained). The conductivities for surface estimation were set to default (scalp 1, skull 0.0125, brain 1). With the aim of avoiding

curse of dimensionality in the inverse problem of EEG-source localization, we choose to employ a standard brain volume partition in which the brain volume itself is divided into a number of region of interest (ROI) defined according to anatomical and functional criteria. Among the different available standard ROI partitions of the brain volume, also called brain atlases, we employed the automated-anatomical labelling (AAL) atlas for a total of 95 brain ROIs (Tzourio-Mazoyer et al., 2002). This choice was due to AAL large use and acknowledgement in the field, as well as for the comparable cardinality of the atlas (i.e., 95 ROIs) with respect to the number of EEG electrodes (i.e., 128). The present study does not delve into the anatomical and structural differences among standard ROI partitions and their functional consequences, but an interested reader may find material in (Evans et al., 2012). Sources were visualized using the ggseg package for R (https://www.r-project.org/) and AAL implementations (Rolls et al., 2015).

The source spectrogram was computed for ROIs by averaging the time-varying vertices using a short-time Fourier transform with a Hanning taper. Calculations were performed through a 2s sliding time window with a 50% overlap, resulting in spectrogram resolutions of 1s and 0.5Hz. The power spectral density (PSD) time series were then integrated within five canonical frequency bands (delta: $\delta \in [1-4]$ Hz, theta: $\theta \in [4-8]$ Hz, alpha: $\alpha \in [8-12]$ Hz, beta: $\beta \in [12-30]$ Hz, and gamma: $\gamma \in [30-45]$ Hz).

2.4 | ECG processing

The ECG time series was bandpass filtered using a Butterworth filter of order 4, between 0.5 and 45 Hz. The R-peaks from the QRS waves were first identified via an automatized process, followed by a visual inspection of misdetections and final automated correction of the remaining misdetections or ectopic heartbeats. This procedure is based on a template-based method for detecting R peaks (Candia-Rivera et al., 2021). All detected peaks were visually inspected over the original ECG along with an interbeat interval histogram. Manual corrections were performed where needed and then automatic corrections were done using a point-process algorithm (Citi et al., 2012).

After cubic interpolation of HRV series at 4Hz, the time-resolved spectogram of the HRV series was estimated using the smoothed pseudo-Wigner–Ville distribution integrated into the two classical intervals 0.04–0.15Hz (i.e., low-frequency band LF) as a non-specific marker of sympathovagal activity and in the range 0.15–0.4Hz (i.e., high-frequency band HF) for parasympathetic activity. We also considered a third interval $0.1-0.2$ Hz (i.e., intermediate frequency IF) to account for the HRV oscillations known to exists centered around 0.15Hz (Klimesch, 2018; Kluger & Gross, 2020; Perlitz et al., 2004; Pfurtscheller et al., 2022). Such an IF band may be practical for studying the BHI (Keller et al., 2020) and its relation to respiratory sinus arrhythmia and baroreflex mechanism (Eckberg, 2009; Julien, 2006).

The three power series derived from HRV (i.e., LF, IF, and HF) were sampled at 1Hz to be homogeneous with those derived from the source estimation.

2.5 | Intracortical brain-heart interplay estimation

As the first attempt to estimate BHI at the brain source level, we conducted a functional correlation analysis using the Spearman method between the time-resolved PSD from the source ROI and cardiovascular dynamics.

To obtain an intersubject BHI measure, each PSD series (i.e., related to a specific experimental phase, brain- and HRV-related frequency bands, and ROI) was constructed by concatenating the subject-specific PSD series. To level the intersubject range difference, each subject-specific PSD series was z-scored before concatenation. Eventually, each series counted 60 (time instants) × 26 (subject) points for the first dataset, and 60 (time instants) × 34 (subject) points for the second dataset.

Finally, Spearman's correlation coefficients were calculated for each HRV-PSD time series (i.e., LF, IF, and HF) and each band-specific ROI-PSD series (i.e., $\delta, \theta, \alpha, \beta, \gamma$). To statistically assess significance of the correlation coefficients, the associated p-values were calculated through a Z-test, due to the large sample size. The significance threshold was fixed at 0.05, and p-value correction for multiple comparisons was accounted for using the Bonferroni–Holm correction over the 95 source ROIs. Detailed statistical description of the correction applied can be found at (Abdi, 2010).

The entire processing procedure pipeline is illustrated in Figure 1.

3 | RESULTS

The experimental results were expressed in terms of Spearman's correlation coefficient and associated p-values as calculated per ROI and EEG- and HRV-derived frequency bands. To provide an overview of the findings, Figure 2 is a radar chart of the number of significant correlations detected in the resting state (upper plot) and CPT phase (lower plot), for both LF (blue), IF (orange), and HF (yellow), in the analysis of dataset D1. Each vertex of the radar chart represents a specific brain-associated frequency band (i.e., $\delta, \theta, \alpha, \beta, \gamma$) for the 95 ROIs.

As shown in the top panel of Figure 2, during the resting state, no significant correlations were detected within the IF and HF cardiovascular bands, as well as within a higher frequency range of the EEG-sources spectrum (i.e., α, β, γ bands), which encompassed frequencies above 8Hz. Notably, significant correlations were primarily detected in $\delta-$LF combination, comprising a third of the ROIs (32 of 95), and $\theta-$LF relationship with 12 significant ROIs out of 95. Complementary to this, during the CPT phase, as depicted in the lower panel of Figure 2, no significant correlations were detected when considering the IF and HF cardiovascular bands, whereas a notably higher number of regions showed significant correlations with the LF cardiovascular component as compared to the resting state. Specifically, nearly the entire set of ROIs exhibited a significant correlation with the LF band, considering both the δ and γ frequency bands (i.e., 84 and 81 of 95 ROIs, respectively), 46 of 95 ROIs were highlighted in the β band, and 31 of 95 ROIs were highlighted in the θ band.
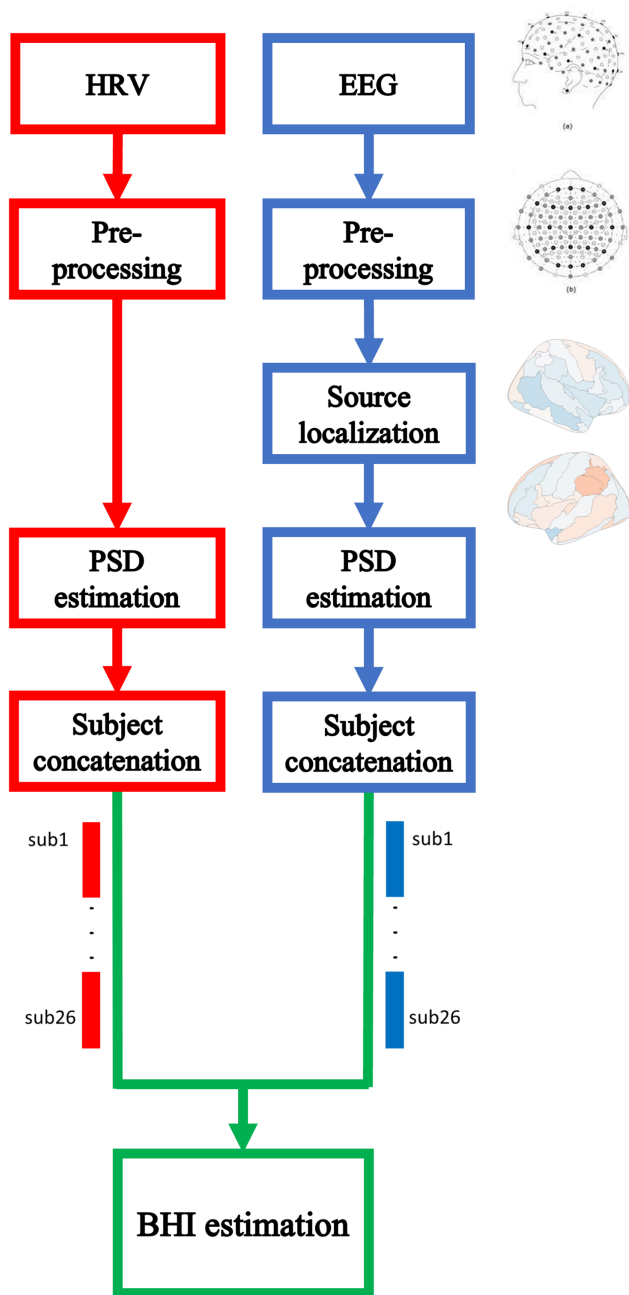
FIGURE 1 Graphical representation of the processing pipeline.

As previously mentioned, to better assess robustness of the method a second dataset (D2) has been analysed comprising a resting state, and the experimental results are presented in Figure 3. As in the resting state of dataset D1, no significant correlations were detected within the IF and HF cardiovascular bands with all EEG bands exception given for the γ band. Similarly, no significant Spearman correlation were detected within the HRV-LF band. The only significant value reported are related to the HRV-HF (10 of 95 ROIs) and HRV-IF (22 of 95 ROIs) with the EEG-γ band. Experimental results from the analysis of the two different datasets are largely in agreement, even if they show some differences. The relations that were the only significant in dataset D1 were absent in D2, whereas in dataset D2 some

significant correlations were found in $\gamma - $IF combination. Considering the limited amount of data in both datasets, a disagreement of this range could be expected, and it is encouraging that in an overwhelming part of combinations of ROIs, and sources- and HRV- frequency bands there is agreement between the two different datasets.

As a further investigation of the specific locations of the significant correlations observed and the quantitative evaluation of this BHI estimation, Figure 4 graphically represents most of the significant correlation coefficients, particularly related to dataset D1. The three most enhanced combinations of frequency bands were HRV-LF and EEG sources in the δ, β, and γ ranges. The other frequency ranges (sources θ and α, HRV-HF, as well as the significant regions found in dataset D2) are reported in Figures 1–3 of the Supplementary Material, respectively. Specifically, Figure 4 comprises six subpanels organized as follows: the two columns are associated with two experimental phases (i.e., the resting state on the left and CPT on the right), whereas the three rows are associated with the frequency bands of the three sources. Subpanels were generated using R-Studio[1] software and the ggseg[2] package, and represent the right hemisphere in the first row (the left hemisphere is in the second row), for both the lateral (left column) and medial (right column) views.

Figure 4 graphically represents the varying numbers of significant regions reported in Figure 2. We can now appreciate that all the regions that are significant in the $\delta - $LF interplay during the resting state hold their significance during CPT, with the addition of various other ROIs. In the resting state, a significant $\delta - $LF BHI was detected on a belt spanning the left lateral hemisphere from the frontal to dorso-parietal area. Additionally, a narrower portion was observed in the right hemisphere, and a few regions on the medial frontal lobes and an area in the left dorso-parietal region also presented significant correlations. During the CPT phase, the $\delta - $LF interplay showed significance across the cortex, except for the central-medial region in both hemispheres, which was more pronounced on the left side.

Conversely, the $\beta - $LF and $\gamma - $LF BHI did not reveal significant areas during the resting state, except for a small left temporal region for the $\beta - $LF relationship. However, these became more prominent during the CPT phase. Specifically, both the lateral and medial frontal regions in both hemispheres as well as the right temporal lobe and a region encompassing the left dorso-temporal and occipital areas exhibited significance in both β and γ frequency bands. While the β band does not exhibit any other ROI, the γ band increases its significance by covering nearly the entire left hemisphere, leaving only a centro-parietal region on the right hemisphere unaffected.

Interestingly, all detected correlations showed a positive sign, indicating that an increasing trend in one of the PSDs involved (e.g., the sources' γ-band) corresponds to a homogeneous trend in the HRV-LF series.

For a detailed list of the specific ROIs correlated with HRV-LF dynamics, please refer to Table 1 in the Supplementary Material. We can appreciate the significant correlations detected between source-δ

---

[1]https://posit.co/download/rstudio-desktop/
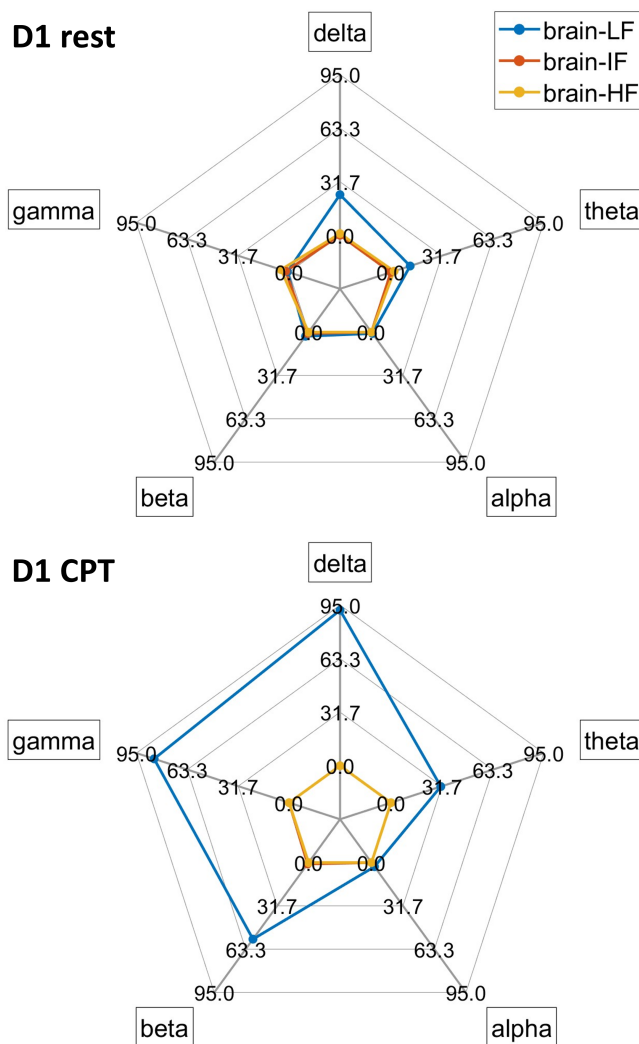[2]https://github.com/ggseg

D1 rest

D2 rest

FIGURE 3 Radar chart representation of the number of ROIs having significant correlations with HRV-LF (blue lines), HRV-IF (orange lines), or HRV-HF (yellow lines) during the resting state of dataset D2. Each vertex of the charts refers to a specific brain-associated frequency band (i.e., $\delta, \theta, \alpha, \beta, \gamma$).

D1 CPT

FIGURE 2 Radar chart representation of the number of ROIs having significant correlations with HRV-LF (blue lines), HRV-IF (orange lines), or HRV-HF (yellow lines) during the resting state (upper panel) and CPT phase (lower panel) of dataset D1. Each vertex of the charts refers to a specific brain-associated frequency band (i.e., $\delta, \theta, \alpha, \beta, \gamma$).

and -γ and HRV-LF, particularly in specific CAN regions, such as insula, amygdala, anterior and middle cingulum, hippocampus, and thalamus. For the sake of completeness, Tables 2 and 3 of the Supplementary Material report a detailed list of the corrected p-value related to all the sources- and HRV- frequency band combinations for the ROIs considered.

4 | DISCUSSION

In this study, a novel approach to investigate the BHI phenomenon at the brain source level was introduced. The BHI was estimated using Spearman's correlation between the brain source electrical activity (derived through sLORETA technique) and cardiovascular dynamics, both estimated through th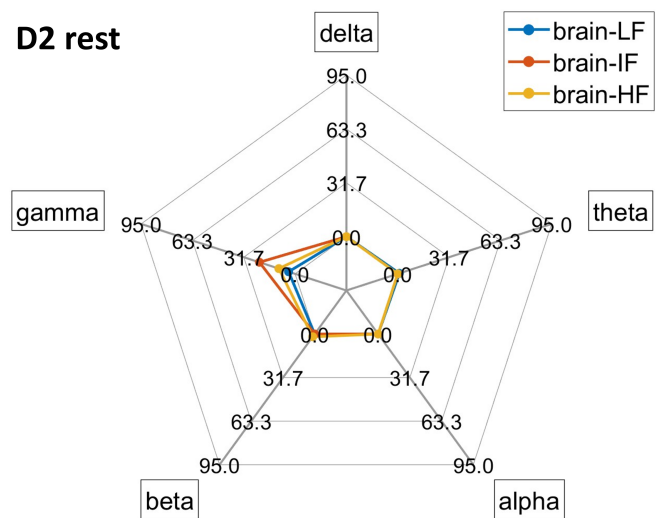eir PSD representation, separated into canonical frequency bands. To validate the methodological approach, an experimental dataset comprising recordings from 26 subjects during the resting state and a strong sympathovagal elicitation, such as CPT, was employed. The experimental results revealed that several brain regions exhibited significant correlations with HRV activity. Interestingly, the nature of these correlations varies depending on the experimental phase and frequency band considered.

From a methodological viewpoint, the proposed approach marks an advancement in the spatial specificity of the BHI estimation. This represents a noteworthy step away from the spatial constraints typically observed in the development of biomarkers based on EEG. This approach can pave the way for further developments in the localization of BHI while preserving the time-frequency resolution of electrophysiological analysis. However, it is worth noting that EEG-based source localization does not reach the spatial resolution provided by fMRI, and represents an indirect extrapolation of the measure of inner CNS region activity. Nevertheless, source localization techniques have achieved a reliable level of accuracy in the reconstruction of brain dynamics. The time resolution achieved by these techniques, which we have only partially explored, may help further develop the BHI research field.

From a physiological viewpoint, the results presented in this study further deepen our knowledge of BHI under sympathovagal elicitation. Our findings revealed a notable increase in the number of ROIs that showed correlations with LF-HRV, a feature often linked to cardiac sympathetic activity, albeit subject to debate. Furthermore, we identified a significant correlation specifically during CPT. This correlation has been observed in regions frequently associated with cardiac autonomic regulation, including the insula, anterior and midcingulate cortices, amygdala, thalamus, and hippocampus (Mazzola et al., 2023). The significant correlation detected in the resting state, mainly at low

FIGURE 4 Graphical representation of the significant correlation coefficient. The left column refers to the resting state period and the right to the CPT phase. On the left side of each column, the frequency bands involved are expressed for both the brain and heart. Each subpanel has two rows and two columns: the first row is the right hemisphere, the second row represents the left hemisphere, whereas left column is the lateral view and the right column represents the medial view.
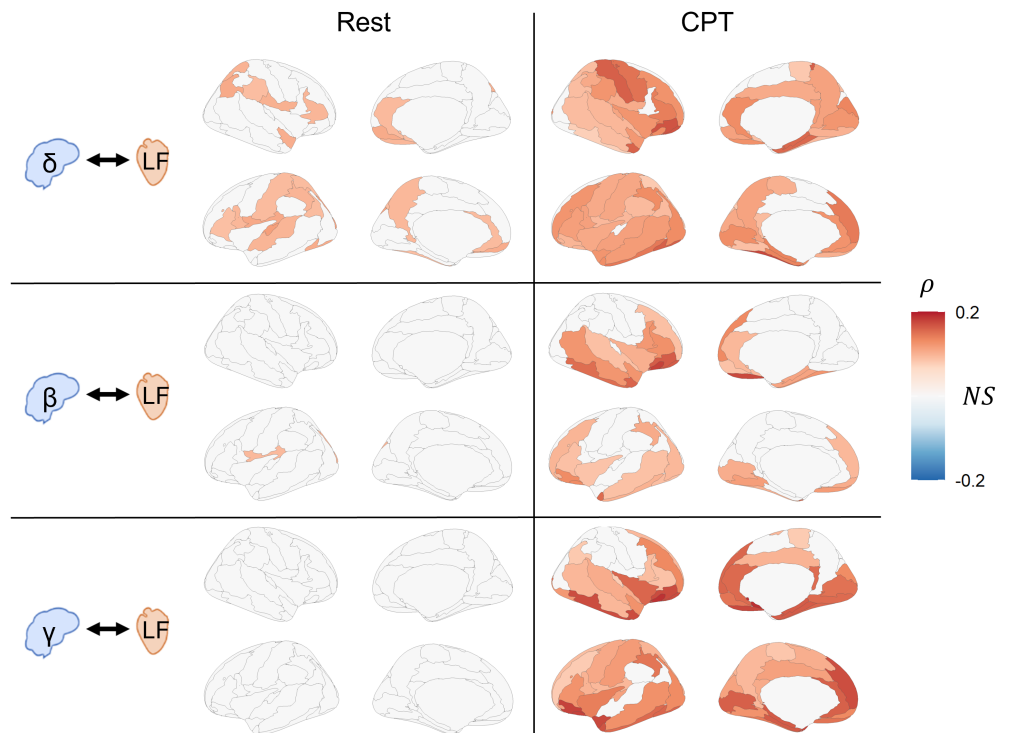
frequencies (i.e., EEG-δ and HRV-LF), can be interpreted within the framework of the Mayer wave phenomenon. These are transient oscillatory responses to hemodynamic perturbations (Julien, 2006), suggesting that a central pacemaker is present at low frequencies (Pfurtscheller et al., 2017; Pfurtscheller et al., 2020; Pfurtscheller et al., 2022). In this framework, heartbeat and breathing dynamics might induce the pressure pulsatility to which the mechano-sensitive pyramidal neurons responds in a frequency range belonging to the δ band (Hamill, 2023; Klimesch, 2023). Moreover, the absence of correlation with the higher frequency bands of the HRV series may be attributed to the specificity of CPT stimuli, which act as physical stressors and may elicit specific changes other than other cognitive stressors (Candia-Rivera et al., 2023; Young & Benton, 2015).

CPT is an interesting elicitation protocol since it represents a complex of concurrent stimulations: somatosensory, via the thermal stress and sub-threshold pain; emotional, since the perception raises a certain arousal and valence; and motor, by holding the hand in an unpleasant state, requiring strong voluntary motor control. These stimuli arouse concurrent and partially independent CNS and ANS responses, meaning that both systems are affected by their specific activities, as well as by their inter-system communication. Among the expected ANS-specific effects elicited by CPT are the baroreceptor modulation of heart rate due to physiological arousal (Cui et al., 2002) and the decreased heart-beat evoked potentials under cold stimuli, mainly over the frontal and central scalp locations (Shao et al., 2011). It is noteworthy that CPT involves physiological signaling from the skin to the brain. These physiological dynamics have been captured through physiological modeling of the BHI, in which the ascending BHI information flow (i.e., heart-to-

brain) is the first response to the CPT stimulus, which is followed by the descending flow (Candia-Rivera, Catrambone, Barbieri, & Valenza, 2022). Interestingly, these results are consistent with those reported in high-arousal conditions, such as emotional elicitation (Candia-Rivera et al., 2023; Candia-Rivera, Catrambone, Thayer, et al., 2022), suggesting a leading role for BHI in the physiology of arousal. The current study, even without investigating the timing and direction of the interaction, supports the literature on the brain frequency bands involved in the BHI (Candia-Rivera, Catrambone, Barbieri, & Valenza, 2022; Catrambone et al., 2019), mainly δ and γ, and bridges fMRI and electrophysiological studies pointing at the CAN as the main player in CNS and ANS interaction (Benarroch, 2012; Valenza et al., 2019).

This study had some limitations. First, in this primary study estimating BHI in the EEG source space, we utilized a basic model-free analysis relying on Spearman's correlations and predominantly employed the general sLORETA technique for solving the source localization inverse problem. However, more specific computational models are required to better catch the BHI dynamics as a whole, including its temporal dynamics, nonlinearity, and directionality, both in terms of interplay estimation and source localization. For instance, sLORETA is known to have relatively coarse spatial resolution, which becomes particularly significant when addressing source localization at a microscopic scale. Nevertheless, this study focused on a partition of the brain volume in agglomerated ROIs, thus maintaining a macroscopic scale. Moreover, the proposed methodology does not consider potential confounding factors related to physiological variables such as respiration or blood pressure. Specifically, relationships have been found between respiration and spectral content of hippocampal

activity in mice (Bagur et al., 2021), rodents, and human patients (Herrero et al., 2018; Zelano et al., 2016). Furthermore, the proposed processing pipeline is susceptible to specific limitations, especially linked to the nonspecificity of HRV power as well as the source localization procedure. More advanced techniques will be employed in future studies to develop a source-related BHI framework for application in larger cohorts. Finally, actual temperature of the hand was not measured before and after the CPT.

5 | CONCLUSION

In conclusion, we here proposed an approach for estimating the functional relationship between the activity of specific brain regions and cardiovascular dynamics during strong sympathovagal elicitation using noninvasive recordings. This approach holds promise for investigating the interplay between the brain and heart with high-time resolution in flexible ecological setups without renouncing spatial information. Our results indicate that intracortical BHI increases during CPT with respect to resting state, mainly targeting neural oscillations in the θ, β, and γ bands.

AUTHOR CONTRIBUTIONS

V.C., D.C.R., and G.V. designed the research; V.C., D.C.R., and G.V. performed the research; V.C. and D.C.R. analyzed the data; and V.C., D.C.R., and G.V. wrote the paper.

FUNDING INFORMATION

CONFLICT OF INTEREST STATEMENT

The authors declare that they have no competing financial interests or personal relationships that may have influenced the work reported in this study.

DATA AVAILABILITY STATEMENT

This study was approved by the local ethics committee of the Area Vasta Nord-Ovest Toscana. The participants signed an informed consent form to participate in the study, as required by the Declaration of Helsinki. None of the participants had any history of neurological, cardiovascular, or respiratory diseases. Raw data of dataset 2 are freely available (Averta et al., 2021) and raw data of dataset 1 are freely available through reasonable mail requests if the ethical requirements are met.

ORCID

Vincenzo Catrambone https://orcid.org/0000-0001-9030-7601
Diego Candia-Rivera https://orcid.org/0000-0002-4043-217X
Gaetano Valenza https://orcid.org/0000-0001-6574-1879

REFERENCES

Abdi, H. (2010). Holm's sequential bonferroni procedure. *Encyclopedia of Research Design*, *1*(8), 1–8.

Antonacci, Y., Barà, C., Zaccaro, A., Ferri, F., Pernice, R., & Faes, L. (2023). Time-varying information measures: An adaptive estimation of information storage with application to brain-heart interactions. *Frontiers in Network Physiology*, *3*, 1242505.

Asadzadeh, S., Rezaii, T. Y., Beheshti, S., Delpak, A., & Meshgini, S. (2020). A systematic review of eeg source localization techniques and their applications on diagnosis of brain abnormalities. *Journal of Neuroscience Methods*, *339*, 108740.

Averta, G., Barontini, F., Catrambone, V., Haddadin, S., Handjaras, G., Held, J. P., Hu, T., Jakubowitz, E., Kanzler, C. M., Kühn, J., Lambercy, O., Leo, A., Obermeier, A., Ricciardi, E., Schwarz, A., Valenza, G., Bicchi, A., & Bianchi, M. (2021). U-limb: A multi-modal, multi-center database on arm motion control in healthy and post-stroke conditions. *GigaScience*, *10*(6), giab043.

Babo-Rebelo, M., Wolpert, N., Adam, C., Hasboun, D., & Tallon-Baudry, C. (2016). Is the cardiac monitoring function related to the self in both the default network and right anterior insula? *Philosophical Transactions of the Royal Society of London. Series B, Biological Sciences*, *371*(1708), 20160004.

Bagur, S., Lefort, J. M., Lacroix, M. M., de Lavilléon, G., Herry, C., Chouvaeff, M., Billand, C., Geoffroy, H., & Benchenane, K. (2021). Breathing-driven prefrontal oscillations regulate maintenance of conditioned-fear evoked freezing independently of initiation. *Nature Communications*, *12*(1), 2605.

Barà, C., Zaccaro, A., Antonacci, Y., Dalla Riva, M., Busacca, A., Ferri, F., Faes, L., & Pernice, R. (2023). Local and global measures of information storage for the assessment of heartbeat-evoked cortical responses. *Biomedical Signal Processing and Control*, *86*, 105315.

Benarroch, E. E. (1993). The central autonomic network: Functional organization, dysfunction, and perspective. In *Mayo clinic proceedings* (Vol. 68, pp. 988–1001). Elsevier.

Benarroch, E. E. (2012). Central autonomic control. In *Primer on the autonomic nervous system* (pp. 9–12). Elsevier.

Candia-Rivera, D. (2023). Modeling brain-heart interactions from Poincaré plot-derived measures of sympathetic-vagal activity. *MethodsX*, *10*, 102116.

Candia-Rivera, D., Catrambone, V., Barbieri, R., & Valenza, G. (2022). Functional assessment of bidirectional cortical and peripheral neural control on heartbeat dynamics: A brain-heart study on thermal stress. *NeuroImage*, *251*, 119023.

Candia-Rivera, D., Catrambone, V., Thayer, J. F., Gentili, C., & Valenza, G. (2022). Cardiac sympathetic-vagal activity initiates a functional brain–body response to emotional arousal. *Proceedings of the National Academy of Sciences*, *119*(21), e2119599119.

Candia-Rivera, D., Catrambone, V., & Valenza, G. (2021). The role of electroencephalography electrical reference in the assessment of functional brain–heart interplay: From methodology to user guidelines. *Journal of Neuroscience Methods*, *360*, 109269.

Candia-Rivera, D., Norouzi, K., Ramsøy, T. Z., & Valenza, G. (2023). Dynamic fluctuations in ascending heart-to-brain communication under mental stress. *American Journal of Physiology-Regulative, Integrative and Comparative Physiology*, *324*(4), R513–R525.

Catrambone, V., Averta, G., Bianchi, M., & Valenza, G. (2021). Toward brain-heart computer interfaces: A study on the classification of upper limb movements using multisystem directional estimates. *Journal of Neural Engineering*, *18*(4), 046002.

Catrambone, V., Greco, A., Vanello, N., Scilingo, E. P., & Valenza, G. (2019). Time-resolved directional brain-heart interplay measurement through synthetic data generation models. *Annals of Biomedical Engineering*, *47*, 1479–1489.

Catrambone, V., Talebi, A., Barbieri, R., & Valenza, G. (2021). Time-resolved brain-to-heart probabilistic information transfer estimation

using inhomogeneous point-process models. *IEEE Transactions on Biomedical Engineering*, 68(11), 3366–3374.

Catrambone, V., & Valenza, G. (2021). *Functional brain-heart interplay*. Springer.

Catrambone, V., & Valenza, G. (2023a). Complex brain-heart mapping in mental and physical stress. *IEEE Journal of Translational Engineering in Health and Medicine*, 11, 495–504.

Catrambone, V., & Valenza, G. (2023b). Nervous-system-wise functional estimation of directed brain–heart interplay through microstate occurrences. *IEEE Transactions on Biomedical Engineering*, 70, 2270–2278.

Chang, P. F., Arendt-Nielsen, L., & Chen, A. C. (2002). Dynamic changes and spatial correlation of eeg activities during cold pressor test in man. *Brain Research Bulletin*, 57(5), 667–675.

Chen, W. G., Schloesser, D., Arensdorf, A. M., Simmons, J. M., Cui, C., Valentino, R., Gnadt, J. W., Nielsen, L., Hillaire-Clarke, C. S., Spruance, V., Horowitz, T. S., Vallejo, Y. F., & Langevin, H. M. (2021). The emerging science of Interoception: Sensing, integrating, interpreting, and regulating signals within the self. *Trends in Neurosciences*, 44(1), 3–16.

Citi, L., Brown, E. N., & Barbieri, R. (2012). A real-time automated point-process method for the detection and correction of erroneous and ectopic heartbeats. *IEEE Transactions on Biomedical Engineering*, 59(10), 2828–2837.

Cui, J., Wilson, T. E., & Crandall, C. G. (2002). Baroreflex modulation of muscle sympathetic nerve activity during cold pressor test in humans. *American Journal of Physiology-Heart and Circulatory Physiology*, 282(5), H1717–H1723.

Dirlich, G., Vogl, L., Plaschke, M., & Strian, F. (1997). Cardiac field effects on the eeg. *Electroencephalography and Clinical Neurophysiology*, 102(4), 307–315.

Eckberg, D. L. (2009). Point: Counterpoint: Respiratory sinus arrhythmia is due to a central mechanism vs. respiratory sinus arrhythmia is due to the baroreflex mechanism. *Journal of Applied Physiology*, 106, 1740–1742.

Evans, A. C., Janke, A. L., Collins, D. L., & Baillet, S. (2012). Brain templates and atlases. *NeuroImage*, 62(2), 911–922.

Faes, L., Marinazzo, D., Jurysta, F., & Nollo, G. (2015). Linear and nonlinear brain–heart and brain–brain interactions during sleep. *Physiological Measurement*, 36(4), 683–698.

Fardo, F., Vinding, M. C., Allen, M., Jensen, T. S., & Finnerup, N. B. (2017). Delta and gamma oscillations in operculo-insular cortex underlie innocuous cold thermosensation. *Journal of Neurophysiology*, 117(5), 1959–1968.

Gabard-Durnam, L. J., Mendez Leal, A. S., Wilkinson, C. L., & Levin, A. R. (2018). The harvard automated processing pipeline for electroencephalography (happe): Standardized processing software for developmental and high-artifact data. *Frontiers in Neuroscience*, 12, 97.

Hamill, O. P. (2023). Pressure pulsatility links cardio-respiratory and brain rhythmicity. *Journal of Integrative Neuroscience*, 22(6), 143.

Herrero, J. L., Khuvis, S., Yeagle, E., Cerf, M., & Mehta, A. D. (2018). Breathing above the brain stem: Volitional control and attentional modulation in humans. *Journal of Neurophysiology*, 119, 145–159.

Julien, C. (2006). The enigma of mayer waves: Facts and models. *Cardiovascular Research*, 70(1), 12–21.

Keller, M., Pelz, H., Perlitz, V., Zweerings, J., Röcher, E., Baqapuri, H. I., & Mathiak, K. (2020). Neural correlates of fluctuations in the intermediate band for heart rate and respiration are related to interoceptive perception. *Psychophysiology*, 57(9), e13594.

Klimesch, W. (2018). The frequency architecture of brain and brain body oscillations: An analysis. *European Journal of Neuroscience*, 48(7), 2431–2453.

Klimesch, W. (2023). Heartbeat, brain oscillations and body awareness: A commentary. *Journal of Integrative Neuroscience*, 22(6), 155.

Kluger, D. S., & Gross, J. (2020). Depth and phase of respiration modulate cortico-muscular communication. *NeuroImage*, 222, 117272.

Liu, W., Zhang, X., Wu, Z., Huang, K., Yang, C., & Yang, L. (2022). Brain–heart communication in health and diseases. *Brain Research Bulletin*, 183, 27–37.

Marina, N., Teschemacher, A. G., Kasparov, S., & Gourine, A. V. (2016). Glia, sympathetic activity and cardiovascular disease. *Experimental Physiology*, 101(5), 565–576.

Mazzola, L., Mauguière, F., & Chouchou, F. (2023). Central control of cardiac activity as assessed by intra-cerebral recordings and stimulations. *Neurophysiologie Clinique*, 53(2), 102849.

Michel, C. M., & He, B. (2019). Eeg source localization. *Handbook of Clinical Neurology*, 160, 85–101.

Oostenveld, R., Fries, P., Maris, E., & Schoffelen, J.-M. (2011). Fieldtrip: Open source software for advanced analysis of meg, eeg, and invasive electrophysiological data. *Computational Intelligence and Neuroscience*, 2011, 1–9.

Park, H.-D., Bernasconi, F., Salomon, R., Tallon-Baudry, C., Spinelli, L., Seeck, M., Schaller, K., & Blanke, O. (2018). Neural sources and underlying mechanisms of neural responses to heartbeats, and their role in bodily self-consciousness: An intracranial EEG study. *Cerebral Cortex*, 28(7), 2351–2364.

Park, H.-D., & Blanke, O. (2019). Heartbeat-evoked cortical responses: Underlying mechanisms, functional roles, and methodological considerations. *NeuroImage*, 197, 502–511.

Pascual-Marqui, R. D., Michel, C. M., & Lehmann, D. (1994). Low resolution electromagnetic tomography: A new method for localizing electrical activity in the brain. *International Journal of Psychophysiology*, 18(1), 49–65.

Pascual-Marqui, R. D. (2002). Standardized low-resolution brain electromagnetic tomography (sloreta): Technical details. *Methods and Findings in Experimental and Clinical Pharmacology*, 24(Suppl D), 5–12.

Perlitz, V., Lambertz, M., Cotuk, B., Grebe, R., Vandenhouten, R., Flatten, G., Petzold, E. R., Schmid-Schönbein, H., & Langhorst, P. (2004). Cardiovascular rhythms in the 0.15-Hz band: Common origin of identical phenomena in man and dog in the reticular formation of the brain stem? *Pflügers Archiv*, 448, 579–591.

Pfurtscheller, G., Blinowska, K. J., Kaminski, M., Rassler, B., & Klimesch, W. (2022). Processing of fmri-related anxiety and information flow between brain and body revealed a preponderance of oscillations at 0.15/0.16 Hz. *Scientific Reports*, 12(1), 9117.

Pfurtscheller, G., Schwerdtfeger, A. R., Rassler, B., Andrade, A., Schwarz, G., & Klimesch, W. (2020). Verification of a central pacemaker in brain stem by phase-coupling analysis between hr interval- and bold-oscillations in the 0.10–0.15 Hz frequency band. *Frontiers in Neuroscience*, 14, 922.

Pfurtscheller, G., Schwerdtfeger, A. R., Seither-Preisler, A., Brunner, C., Aigner, C. S., Brito, J., Carmo, M. P., & Andrade, A. (2017). Brain–heart communication: Evidence for "central pacemaker" oscillations with a dominant frequency at 0.1 Hz in the cingulum. *Clinical Neurophysiology*, 128(1), 183–193.

Rolls, E. T., Joliot, M., & Tzourio-Mazoyer, N. (2015). Implementation of a new parcellation of the orbitofrontal cortex in the automated anatomical labeling atlas. *NeuroImage*, 122, 1–5.

Schiecke, K., Pester, B., Piper, D., Benninger, F., Feucht, M., Leistritz, L., & Witte, H. (2016). Nonlinear directed interactions between hrv and eeg activity in children with tle. *IEEE Transactions on Biomedical Engineering*, 63(12), 2497–2504.

Shao, S., Shen, K., Wilder-Smith, E. P., & Li, X. (2011). Effect of pain perception on the heartbeat evoked potential. *Clinical Neurophysiology*, 122(9), 1838–1845.

Shao, S., Shen, K., Yu, K., Wilder-Smith, E. P., & Li, X. (2012). Frequency-domain eeg source analysis for acute tonic cold pain perception. *Clinical Neurophysiology*, 123(10), 2042–2049.

Silvani, A., Calandra-Buonaura, G., Dampney, R. A., & Cortelli, P. (2016). Brain–heart interactions: Physiology and clinical implications.

Philosophical Transactions of the Royal Society A: Mathematical, Physical and Engineering Sciences, 374(2067), 20150181.

Skora, L. I., Livermore, J. J. A., & Roelofs, K. (2022). The functional role of cardiac activity in perception and action. *Neuroscience & Biobehavioral Reviews, 137*, 104655.

Tadel, F., Baillet, S., Mosher, J. C., Pantazis, D., & Leahy, R. M. (2011). Brainstorm: A user-friendly application for meg/eeg analysis. *Computational Intelligence and Neuroscience, 2011*, 1–13.

Truter, N., Malan, L., & Essop, M. F. (2023). Glial cell activity in cardiovascular diseases and risk of acute myocardial infarction. *American Journal of Physiology-Heart and Circulatory Physiology, 324*(4), H373–H390.

Tzourio-Mazoyer, N., Landeau, B., Papathanassiou, D., Crivello, F., Etard, O., Delcroix, N., Mazoyer, B., & Joliot, M. (2002). Automated anatomical labeling of activations in spm using a macroscopic anatomical parcellation of the mni mri single-subject brain. *NeuroImage, 15*(1), 273–289.

Valenza, G., Di Ciò, F., Toschi, N., & Barbieri, R. (2024). Sympathetic and parasympathetic central autonomic networks. *Imaging Neuroscience, 2*, 1–17.

Valenza, G., Passamonti, L., Duggento, A., Toschi, N., & Barbieri, R. (2020). Uncovering complex central autonomic networks at rest: A functional magnetic resonance imaging study on complex cardiovascular oscillations. *Journal of the Royal Society Interface, 17*(164), 20190878.

Valenza, G., Sclocco, R., Duggento, A., Passamonti, L., Napadow, V., Barbieri, R., & Toschi, N. (2019). The central autonomic network at rest: Uncovering functional mri correlates of time-varying autonomic outflow. *NeuroImage, 197*, 383–390.

Young, H., & Benton, D. (2015). We should be using nonlinear indices when relating heart-rate dynamics to cognition and mood. *Scientific Reports, 5*(1), 16619.

Zelano, C., Jiang, H., Zhou, G., Arora, N., Schuele, S., Rosenow, J., & Gottfried, J. A. (2016). Nasal respiration entrains human limbic oscillations and modulates cognitive function. *Journal of Neuroscience, 36*(49), 12448–12467.

SUPPORTING INFORMATION

Additional supporting information can be found online in the Supporting Information section at the end of this article.

How to cite this article: Catrambone, V., Candia-Rivera, D., & Valenza, G. (2024). Intracortical brain-heart interplay: An EEG model source study of sympathovagal changes. *Human Brain Mapping, 45*(6), e26677. https://doi.org/10.1002/hbm.26677